Effects of pH, ionic strength, and temperature on Cs, Ba, Co, and Eu sorption onto biotite: A combined experimental and modeling study

(article starts on next page)

Effects of pH, ionic strength, and temperature on Cs, Ba, Co, and Eu sorption onto biotite: A combined experimental and modeling study

Pawan Kumar [*], Stellan Holgersson, Christian Ekberg

Department of Chemistry and Chemical Engineering, Division of Nuclear Chemistry, Chalmers University of Technology, Kemivägen 4, SE-41296 Göteborg, Sweden

A B S T R A C T

The trace metal sorption onto the phyllosilicate mineral biotite, commonly found in granitic rock, has been studied with batch sorption experiments that were carried out for up to two months. The aim was to investigate the uptake mechanism of the radioisotopes ^{134}Cs, ^{133}Ba, ^{60}Co, and ^{152}Eu at trace concentrations (10^{-8} M) onto crushed biotite at a particle size 0.25–0.5 mm. under inert gas conditions ([O$_2$] < 1 ppm) and to provide data for a Surface Complexation Model. The experiments were conducted in triplicates with the pH adjusted to 5, 6, 7, 8, or 9 with pH-buffered solutions containing either 0.001, 0.01, or 0.1 M NaClO$_4$ at two temperatures: 40 and 60 °C. The results show that the sorption of Cs, Ba, Co and Eu onto biotite are strongly pH-dependent where each element shows a characteristic uptake behavior. The sorption of Cs and Ba appear to be particularly sensitive to increased ionic strength which decreases their sorption while Eu is less affected. In contrast, Co sorption seems to be largely non-affected by change of ionic strength. A temperature increase, on the other hand, has a positive effect on sorption for almost all elements. To estimate the surface acidity constants (pK_a) of biotite at 40 and 60 °C, titration experiments were performed with biotite suspended in solution over a pH range of approximately 3–11. Modeling of the titration data resulted in $pK_{a,1} = -5.0 \pm 0.2$ at 40 °C and -5.3 ± 0.2 at 60 °C. Similarly, $pK_{a,2} = -7.0 \pm 0.3$ at 40 °C and -6.9 ± 0.2 at 60 °C. The sorption data (R_d values) of all metals was successfully modelled with a combination of one amphoteric (2-pK_a) surface complexation site and one ion-exchange site. A non-electrostatic SCM, without any compensation for surface electrostatic effects from electrolyte solution, were used with the reaction constants and coefficients as fitting parameters. From these, the thermodynamic parameters ΔH and ΔS for the sorption reactions were calculated. The results show that surface-complexation reactions are primarily entropy-driven, while ion-exchange reactions are enthalpy-driven.

1. Introduction

In Sweden, nuclear energy has been part of the energy mix for the past 50 years. One of the key challenges associated with nuclear power is the management of high-level radioactive waste (HLW), particularly spent nuclear fuel, due to its significant radiotoxicity. To address this issue, Sweden has adopted a solution involving the direct disposal of spent nuclear fuel in a deep geological repository encased in granite rock (SKB, 2010a) (Hedin and Olsson, 2016). The Swedish Nuclear Fuel and Waste Management Company (SKB), responsible for constructing the repository, has proposed the KBS-3 method. This method employs a multi-barrier storage system, placing copper canisters containing spent nuclear fuel 400–500 m below the surface within granitic rock formations. This approach is designed to securely isolate harmful radionuclides for up to 100,000 years (SKBF/KBS, 1983) (SKB, 2010a) (Hedin

and Olsson, 2016). In safety-case scenarios where the engineered barriers have failed, the bedrock itself constitutes the final barrier to radionuclide migration with groundwater to the biosphere (SKB, 2011). The primary mechanisms that retard radionuclide migration through bedrock fractures are diffusion into the porosity of the rock matrix and sorption onto available mineral surfaces (Neretnieks, 1980), (Grisak and Pickens, 1980), (Ewing, 2015). The sorption behavior of some selected radionuclide elements is the main topic for this study, but this work also has a more general application in the geochemistry field, since the aim is to identify and to introduce a mineral surface chemistry model for the observed sorption behavior.

Radionuclides, such as ^{137}Cs, ^{226}Ra, ^{59}Ni and ^{241}Am are considered among the most safety-critical radionuclides in a repository due to their high abundance in combination with their radiotoxicity and potential long-term risks (SKB, 2010b) (SKB, 2010c). The elements are redox-

insensitive and therefore exist in specific redox states under the repository conditions: Cs(I), Ra(II), Ni(II), and Am(III) (Crawford, 2010). In this work, ^{134}Cs, ^{133}Ba, ^{60}Co, and ^{152}Eu were selected as either primary element of study (Cs) or as analogous element (Ba, Co, and Eu). The sorption of radionuclides under the anticipated repository conditions is typically expressed using the distribution coefficient R_d. Both the Finnish (Posiva) and the Swedish (SKB) nuclear waste management companies have extensively investigated radionuclide sorption onto on-site granitic materials under some limited conditions (Crawford, 2010) (Hakanen et al., 2012). Most results have been released in technical reports like those just cited and some additional studies have appeared in academic publications, some examples are (Allard and Beall, 1979), (Allard et al., 1980), (Skagius et al., 1982), (Ohe, 1984), (Idemitsu et al., 1994), (Murali and Mathur, 2002), (Tsai et al., 2009), (Nebelung and Brendler, 2010), (Fukushi et al., 2013), (Tachi et al., 2015), (Muuri et al., 2016), (Rodionova et al., 2022). However, these studies are mostly empirical and very few of them have modelled R_d on the individual minerals of granitic rock, using surface complexation models (SCMs), which is also the conclusion from a recent literature review (Holgersson and Kumar, 2023).

SCMs provide a more detailed understanding of the sorption processes by describing the interactions occurring at the solid-liquid interface, thereby enhancing the predictive capability of radionuclide retention in granitic rock. Predictions of sorption behavior under different chemical conditions require a reliable sorption model, based on reaction-mechanistic SCM for the individual minerals and then from this, a model of sorption on a complex rock material by methods like the Component Addition approach (Davis et al., 1998), (Davis et al., 2004). Even if geological conditions remain stable within the nuclear waste repository over time, chemical conditions and groundwater composition are likely to be affected by accompanying events to any climate changes, whether it is rising sea-levels or an ingress of fresh water from a de-glaciation phase. Such changes in groundwater composition will lead to changes in R_d values. Granitic rock at the proposed Swedish repository site is composed of many different minerals, including 3 %–12 % biotite (Drake et al., 2006) (Selnert et al., 2008).

Biotite is a solid solution composed primarily of the magnesium-rich endmember phlogopite ($KMg_3(AlSi_3O_{10})(OH)_2$), the iron-endmember annite ($KFe_3^{2+}(AlSi_3O_{10})(OH)_2$), and two more aluminum-rich end-members: siderophyllite ($KFe_2^{2+}Al(Al_2Si_2O_{10})(OH)_2$) and eastonite ($KMg_2Al(Al_2Si_2O_{10})(OH)_2$) (Rieder et al., 1998). Biotite is considered to have a relatively strong radionuclide sorption capacity compared with those of other minerals present in granite (Cornell, 1993), (Tsai et al., 2009) (Fukushi et al., 2013) (Tachi et al., 2015) (Muuri et al., 2016). Therefore, biotite was chosen as the primary mineral for this study.

According to a recent literature review of SCM data for trace element sorption onto biotite (Holgersson and Kumar, 2023) the sorption isotherm study, which involves varying the sorbing element concentration, usually at a fixed pH and ionic strength, is the most commonly used method. Such sorption isotherms have been modelled using a three-site cation-exchange model for Cs sorption (Kyllönen et al., 2014) and for alkaline earth metals such as Ca, Sr and Ra (Söderlund et al., 2019) and Ra (Fabritius et al., 2022), although in the latter the model was re-defined to comprise of one exchange site and two surface complexes sites. The three-site model was originally developed for the clay mineral illite (Bradbury and Baeyens, 2000). At least for Cs sorption, the identification of one weakly sorbing basal sorption site and one strongly sorbing edge site in biotite is also supported by a spectroscopic study (McKinley et al., 2004). According to the same review, systematic studies of radionuclide sorption on biotite under varying conditions, including pH, ionic strength, and temperature, remain limited (Holgersson and Kumar, 2023). In some studies, the pH has been set to a fixed value and the ion strength has been varied (Söderlund et al., 2019) or vice versa (Furuya et al., 1997). Some studies were found in which both the ionic strength and pH were varied while the trace concentrations of Ni and Eu (Puukko et al., 2007) and Eu (Fukushi et al., 2013)

were fixed. These studies were conducted at room temperature, and the sorption data were modelled either using a combination of one 1-pK_a surface complexation site and one ion-exchange site (Puukko et al., 2007) or only one ion-exchange site (Fukushi et al., 2013). Another study was made in a limited range of pH 8–11 with varying Na-carbonate electrolyte concentration for Th sorption onto biotite and sorption was modelled with one 2-pKa surface complexation site only (IIda et al., 2016). This lack of systematic sorption data for biotite is a notable knowledge gap, as it is essential to explore a wider range of variables to develop a robust SCM for a specific mineral (Payne et al., 2013). The aim of this work is to determine the R_d-values for a biotite of well-defined particle size fraction using four radionuclides (^{134}Cs, ^{133}Ba, ^{60}Co, and ^{152}Eu) under varying conditions, including five pH values (5, 6, 7, 8, and 9), three ionic strengths (0.001, 0.01, and 0.1 M NaClO$_4$) and elevated temperatures of 40 and 60 °C. The resulting dataset then serves as an input for obtaining SCM parameters, describing sorption in detail with assigned and specific surface reactions. The modeling method includes PHREEQC geochemical modeling software for speciation calculations, integrated with a computer code written in Python programming language for the parameter optimization. This employs an iterative method (Nelder and Mead, 1965) to derive surface complexation reaction constants and ion-exchange selectivity coefficients. In the same context, a similar study at 25 °C have been reported elsewhere (Cs, Ba, Co, and Eu sorption onto biotite at pH 5–9 and at varying ionic strength, submitted to J. Environ. Radioactiv.).

2. Materials and methods

2.1. Materials and mineral characterization

In this study, a biotite specimen from granitic pegmatite from Risør, Norway was used. In a previous work, the biotite composition was found to be $K_{1.05}(Mg_{0.70}Mn_{0.06}Ti_{0.18}Fe\ (II)_{1.81}Fe\ (III)_{0.25})\ Al_{1.28}Si_{2.62}O_{10}(OH)_2$ (Holgersson et al., 2024). The biotite was prepared for the sorption experiments by crushing it with the help of a blender machine with steel knives (M20, IKA) and then sieving it with stainless steel sieves (200 mm ⌀ ISO3310-1 type, AS200 sieve shaker, Retsch) to achieve a particle size of 0.25–0.5 mm. The resulting material was then washed several times with 95 % ethanol to remove ultrafine particles. The biotite was further dried in a vacuum chamber (Vacucell, MMM) at a temperature of approximately 19±2 °C for several days. The biotite specimen characterization in terms of specific surface area (SSA), acidic site density (ASD), and cation-exchange capacity (CEC) has been previously reported (Cs, Ba, Co, and Eu sorption onto biotite at pH 5–9 and at varying ionic strength, submitted to J. Environ. Radioactiv.). For SSA, Kr gas adsorption was used and evaluated with BET isotherm (Brunauer et al., 1938). For ASD the tritium exchange method (Berubé et al., 1967) was used and for CEC the Na-acetate method (Schollenberger and Simon, 1945) was used. The experimentally obtained SSA, ASD and CEC were determined to be 0.47 ±0.01 m^2/g, 3.3± 0.6 × 10^{-6} mol/g and 1.0 ± 0.1 $cmol_C$/kg, respectively. A concise summary of the experimental methods and findings related to SSA, ASD, and CEC is provided in Appendix C. Impurities, such as Ca^{2+} and Mg$^+$, that are attached to the biotite surface may interfere with batch sorption experiments involving Na$^+$ electrolytes. Therefore, to minimize the influences of other cations, the biotite was converted into a sodium form, containing only Na$^+$ on its exchange sites as much as possible. The procedure has been reported elsewhere (Cs, Ba, Co, and Eu sorption onto biotite at pH 5–9 and at varying ionic strength, submitted to J. Environ. Radioactiv.).

2.2. Titration and batch sorption experiment

Continuous titration on suspensions of biotite in NaClO$_4$ solutions in triplicate was performed to determine the acid-base properties of the biotite mineral at 40 ± 2 °C and 60 ± 2 °C. Standard solutions of 0.01 M

HCl and 0.1 M NaOH (both Titrisol, Merck) were used as titrants, where the latter was prepared and stored in an inert gas glovebox (UNILab, MBraun) to avoid carbonate formation in the solution. A closed glass vessel and computer-controlled automatic titration instrument (905 Titrando, Metrohm) were utilized, as well as a glass electrode (6.0250.010, Metrohm). The vessel temperature was maintained via a water recirculation and heating bath (TC120, Grant). Next, 0.5 g of mineral was added to 50 mL of 0.01 M NaClO$_4$ electrolyte solution. The suspension was stirred for 10 min, and ~ 2.5 mL of HCl solution was added to obtain a pH of approximately 3. The suspension was then titrated with 0.1 M NaOH solution, using a fixed incremental volume of 8 μL/addition in 15 min intervals. Prior to the titrations, the electrode was calibrated to proton concentration by performing the titration procedure proposed by Gran (Gran, 1950). A solid-suspension ratio (S:L) of 1:100 was selected based on the literature recommendations (Jakobsson, 1999), with the aim of balancing the suspension homogeneity and achieving accurate {H$^+$} measurement. Batch sorption experiments were conducted in triplicate at 40±2 °C and 60±2 °C utilizing heating blocks (Isotemp, Fisherbrand) inside a N$_2$-filled glove box (UNILab, Mbraun) with an automatic oxygen-removal system ([O$_2$] < 1 ppm). The radioactive elements used were ^{134}Cs (CsCl in 0.1 M HCl, 10 μg Cs/mL), ^{133}Ba (BaCl$_2$ in 0.1 M HCl, 10 μg Ba/mL), ^{60}Co (CoCl$_2$ in 0.1 M HCl, 10 μg Co/mL), and ^{152}Eu (EuCl$_3$ in 0.5 M HCl, 10 μg Eu/mL) (all provided by Eckert & Ziegler). Three different concentrations of NaClO$_4$ (Merck p.A, >98 %) solutions were prepared: 0.1 M, 0.01 M, and 0.001 M. Each solution was divided into five solutions with different pH values buffered to pH 5–9 using organic pH buffer solutions, as indicated in Table 1, with concentrations of 5 mM for 0.1 M and 0.01 M NaClO$_4$ and 0.5 mM for 0.001 M NaClO$_4$. The buffer solutions were chosen for their negligible tendency to form complexes with metals (Yu et al., 1997).

The pH buffered solution was spiked with a mixture of ^{134}Cs (0.3 MBq/L), ^{133}Ba (0.8 MBq/L), ^{60}Co (0.4 MBq/L), and ^{152}Eu (0.1 MBq/L) corresponding to an approximate concentration of 10^{-8} M for each radionuclide with carrier isotopes included. Then, the solution's pH was re-adjusted using 0.1 M NaOH or HClO$_4$. The pH values were measured with glass electrode and pH meter (pHC 3006–9, pHM 240, Radiometer). The batch sorption experiment was conducted in 10 mL acid-washed polypropylene centrifuge tubes (Oak Ridge 3119–0010, Thermo Scientific) by adding 0.1 g of crushed biotite with 5 mL of radiotracer-spiked NaClO$_4$ solutions, resulting in a solid-to-liquid ratio (S:L) of 1:50. The sorption experiment was completed in approximately two months, where the sampling was done in the time intervals of 2, 14, 28, and 56 days. On each sampling occasion, the tubes were centrifuged at 45,000 g and 0.1 mL samples were withdrawn, except on the last occasion, when the 0.5 mL samples were withdrawn. The gamma count rate per solution volume (cpm/L) of all four radionuclides in the aqueous phase was measured at nuclide-specific gamma energies 121, 356, 605 and 1173 keV for ^{152}Eu, ^{133}Ba, ^{134}Cs and ^{60}Co, respectively, with an HPGe detector equipped with sample changer (GEM23195 detector, 2002C preamp, DSA2000 MCA, GammaAnalyst, Genie2000 v.3.4.1 software, Canberra/Mirion) for 3 h. In total, 90 batch samples were prepared, covering two temperatures, three ionic strengths, and five pH values, each in triplicate. Additionally, 30 blank tubes were prepared to evaluate wall sorption without biotite, along with acidic blanks (0.1 M HCl) in duplicates to determine the reference trace concentration values. Eq. (1) was used to compute the wall sorption-corrected distribution co-efficient R_d (m^3/kg) on biotite for each

radionuclide (Andersson et al., 2008):

$$R_d = \left(\frac{\overline{C} \bullet V_{ref} \bullet V_{out,n}}{A_{out,n}} - \left(V_0 - \sum_{i=1}^{n-1} V_{out,i} \right) - L_d - \frac{V_{out,n} \bullet \sum_{i=1}^{n-1} A_{out,1}}{A_{out,n}} \right) \bullet \frac{1}{m}$$

(1)

Here, the average measured reference concentration $\overline{C}$ (cpm/L) was obtained from the acidic references; $V_{out,n}$ (L) and $A_{out,n}$ (cpm) are the volume and measured activity of sample n, respectively; V_{ref} (L) is the volume of the radioactive solution that was initially added; V_0(L) is initial liquid volume of the batch, including V_{ref} and any remaining liquid from the preconditioning; m (kg) is the mass of the solid used in the sorption experiment; and L_d (L) is a wall sorption factor measured in the blank series of batch tests. The two summation variables in Eq. (1) were derived from an overall mass balance and were used to adjust for radioactivity and the volumes extracted in the subsequent samplings. Essentially the same formula was used to compute the wall sorption factor; however, because the mass involved in wall sorption is unknown, the wall sorption factor L_d (L) can be defined as:

$$R_{d,wall} \bullet m_{wall} = \left(\frac{\overline{C} \bullet V_{ref} \bullet V_{out,n}}{A_{out,n}} - \left(V_0 - \sum_{i=1}^{n-1} V_{out,i} \right) - \frac{V_{out,n} \bullet \sum_{i=1}^{n-1} A_{out,1}}{A_{out,n}} \right)$$
$$\equiv L_d$$

(2)

2.3. Modeling methods for titration and sorption data

The conceptual model used herein to describe sorption on biotite is based on the collected evidence in the literature that at least two distinct types of sorption sites should be present: one on the basal plane surfaces and another at the edges (Nagy, 1995), (Holgersson and Kumar, 2023). The basal plane sites are assumed to be ion-exchange sites, denoted as X, and the edge sites are amphoteric surface complexation sites, denoted as ≡SO$^-$. The conceptualization of the biotite used for modeling is shown in Fig. 1.

In order to apply this model to the measured distribution coefficients R_d at different pH values, one must first make assumptions on some specific surface reactions. The titration data at 40 and 60 °C were modelled by including the following reactions:

$$NaX + H^+ \rightleftharpoons HX + Na^+ \tag{R.1}$$

$$\equiv SOH \rightleftharpoons \ \equiv SO^- + H^+ \tag{R.2}$$

$$\equiv SOH_2 \rightleftharpoons \ \equiv SOH + H^+ \tag{R.3}$$

$$\equiv SO^- + Na^+ \rightleftharpoons \ \equiv SONa \tag{R.4}$$

$$\equiv SOH + Na^+ \rightleftharpoons SOHNa^+ \tag{R.5}$$

These reactions consider ion-exchange on the basal planes between

Table 1

List of organic buffer solutions used in batch sorption experiments.

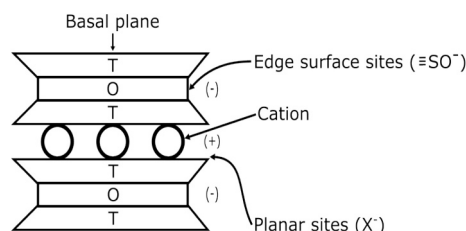| Buffer	pH
DEPP (1,4-Diethylpiperazine, 98 %, Alfa Aesar)	5 and 9
MES (2-(N-Morpholino) ethane sulfonic acid, 99 % Sigma-Aldrich)	6
MOPS (3-(N-Morpholino) propane sulfonic acid, 99.5 % Sigma-Aldrich)	7
PIPPS (1,4-Piperazine bis-(propane sulfonic acid), 98 % Merck)	8

Fig. 1. Graphical representation of the TOT+C structure of the biotite mineral.

the protons and background electrolyte (R.1), protonation of the edge surface (R.2) and (R.3), and strong (R.4) and weak (R.5) surface complexes with the background electrolyte. The corresponding selectivity coefficient for ion exchange K_{NaX} is defined by

$$K_{NaX} = \frac{[HX]\{Na^+\}}{[NaX]\{H^+\}} \tag{3}$$

The surface acidity constants K_{a1} and K_{a2} are defined as

$$K_{a1} = \frac{[\equiv SOH]\{H^+\}}{[\equiv SOH_2]} \tag{4}$$

$$K_{a2} = \frac{[\equiv SO^-]\{H^+\}}{[\equiv SOH]} \tag{5}$$

The surface complexation constants for reactions (R.6) and (R.7) are

$$K_{SONa} = \frac{[\equiv SONa]}{[\equiv SO^-]\{Na^+\}} \tag{6}$$

$$K_{SOHNa} = \frac{[\equiv SOHNa^+]}{[\equiv SOH]\{Na^+\}} \tag{7}$$

The symbol [] indicates that the concentration is given in units of mol/L. In the model, any electrostatic effects from possible charge buildup of electrolyte Na^+ ions on the mineral surface edges were not considered, which means that a non-electrostatic model (NEM) approach was applied. Additional data of total site capacities were taken from the experimental data of ASD and CEC for the surface complexation and ion-exchange, respectively (see Section 2.1). The chemistry speciation calculation for the titration experiment generates a non-linear equation system of four mass balances with the concentration variables $[H^+]$, $[Na^+]$, $[\equiv SO^-]$ and $[HX]$. This speciation calculation was made here with the computer code PHREEQC (Parkhurst and Appelo, 2021), initially with guessed values of the constants in (Eqs. (3)–(7)). Then, the error sum was evaluated:

$$\sum_{i=1}^{n} abs\left([H^+]_{exp,i} - [H^+]_{calc,i}\right) \tag{8}$$

In (Eq. (8)), n is the total number of points in the titration curve, $[H^+]_{exp,i}$ is the measured proton concentration at point i, and $[H^+]_{calc,i}$ is the proton concentration calculated according to the mass balances. The resulting error was minimized with an iterative optimization computer routine written in Python programming language, which guessed values for constants using the Nelder-Mead method (also known as the downhill-Simplex) until the error sum converged to a minimum value (Nelder and Mead, 1965). The communication between the two programs was accomplished with the integration program IPHREEQC (Charlton and Parkhurst, 2011), (Wissmeier and Barry, 2011). After this step, the constants and coefficients in (Eqs. 3–7) were fixed and used in the next step of modeling the sorption distribution coefficients (R_d values) at five different pH values. A similar model was fitted to the equilibrium distribution coefficients R_d in the batch sorption experiments with trace elements and was then used to minimize the error sum:

$$\sum_{i=1}^{n} abs\left(R_{d,exp,i} - R_{d,calc,i}\right) \tag{9}$$

In (Eq. (9)) n denotes the number of batch experiments for one radiotracer and one ionic strength, which were fifteen in total (five pH, made in triplicates). Furthermore, it should be noted that each experimental R_d value is determined for the whole time-dependent series (see Section 3.2), which consists of four sampling points, which altogether gives 60 experimental datapoints for the optimization of the parameters. The optimization was made for the three ionic strengths separately because the ion exchange coefficients tend to vary with ionic strength in a rather unpredictable manner (like R_d coefficients), unlike the reaction constants obtained at zero ionic strength. Similar reactions for ion

exchange (R.1) and surface complexation (R.4 and R.5) were used for the trace element cations. These were modelled individually, assuming the sorption of each element did not interfere with each other. For all elements, except Cs, hydroxide complex formation had to be considered. The aqueous hydroxide complexes included in the model are shown in Table 2, below.

The constants in Table 2 were re-calculated to the appropriate temperature by the PHREEQC database MINTEQ. Some hydroxide complexes of radiotracer were allowed to form ternary surface complexes, and, in some cases, also exchange species. The corresponding reactions with reaction constants and coefficients were defined according to same formalism as for the bare cations. The specific hydroxide complexes that were assumed to partake in sorption are described further in the results (see Tables 6–8). The mass balances for the batch sorption modeling were like those for titration modeling, except that the volume of solution and pH of each individual batch experiment were fixed by initial conditions and then both assumed to be constant. This again generates a non-linear equation system of four mass balances with the concentration variables $[M^+]$, $[Na^+]$, $[\equiv SO^-]$ and $[HX]$, to be solved with the same iterative method as described above. With the reaction constants and coefficients (K is here used for both types) at different temperatures determined, the logarithmic values were then plotted against $1/T$ according to the van't Hoff equation:

$$Log\,K = \frac{\Delta S^o}{R} - \frac{\Delta H^o}{RT} \tag{10}$$

From this, the reaction enthalpies $\Delta H°$ and entropies $\Delta S°$ were evaluated.

3. Results and discussion

3.1. Titration results

The biotite titration results at 40 and 60 °C are shown in Fig. 2, and the corresponding optimized reaction constants for biotite are listed in Table 3.

The changes in pK_a values with temperature indicate that the predominance domain of the non-charged $\equiv SOH$ surface species becomes narrower with increasing temperature, and it seems to favor the charged surface species $\equiv SO^-$ and $\equiv SOH_2^+$. The stability constants for the Na^+ surface complex appear to increase with increasing temperature, which means that Na^+ sorption on sites of this type is favored by increased temperature. Ion exchange between H^+ and Na^+, on the other hand, seems not to be affected by temperature. Fig. 3 shows the net amount of protons consumed as a function of pH at 40 and 60 °C. The point of zero surface charge, pH_{pzc}, is the intersection of the potentiometric titration curves at both temperatures, indicating a value about 5.5–6. Similar results have been reported for other biotite specimen (Puukko et al., 2007).

The experimental CEC and ASD values were adjusted slightly in order to attain an optimal fit of the titration data. The optimized values from titrations are 2.5 and 5.1 times larger than from the CEC and ASD

Table 2
Thermodynamic data at 25 °C and zero ionic strength of aqueous hydroxide complexes of Ba, Co, and Eu used in sorption modeling.

Reaction	log β
$Ba^{2+} + H_2O = Ba(OH)^+ + H^+$	0.68[†]
$Co^{2+} + H_2O = Co(OH)^+ + H^+$	4.39[†]
$Co^{2+} + 2H_2O = Co(OH)_2 + 2H^+$	8.23[†]
$Co^{2+} + 3H_2O = Co(OH)_3^- + 3H^+$	10.0[†]
$Eu^{3+} + H_2O = Eu(OH)^{2+} + H^+$	7.68[‡]
$Eu^{3+} + 2H_2O = Eu(OH)_2^+ + 2H^+$	15.58[‡]
$Eu^{3+} + 3H_2O = Eu(OH)_3^0 + 3H^+$	24.17[‡]

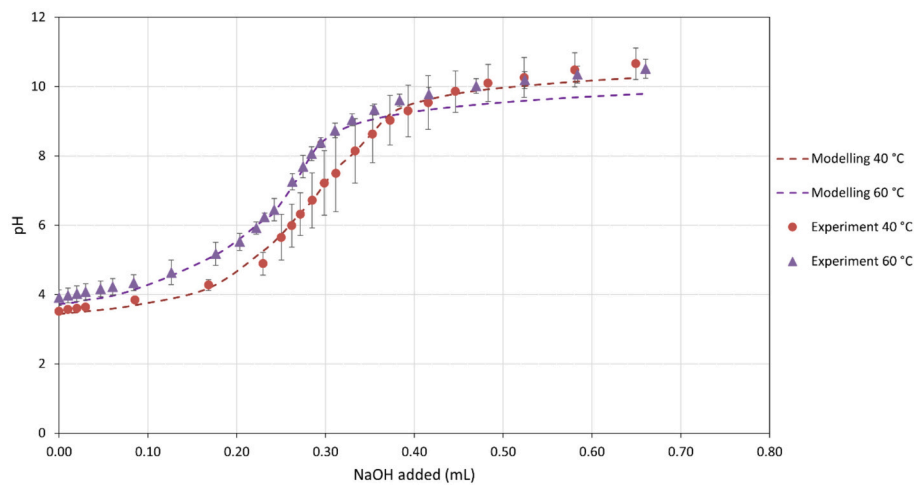from [†] (Ekberg and Brown, 2016) and [‡] (Jordan et al., 2024).

Fig. 2. Experimental (average of triplicates) and modelled titration curves for a suspension of biotite in 0.01 M NaClO$_4$ solution at 40 and 60 °C.

Table 3

Optimized acidity ($\equiv SOH_2$, $\equiv SO^-$), cation-exchange (X), sodium inner ($\equiv SONa$), and sodium outer ($\equiv SOHNa^+$) sphere complex reactions and their associated reaction constants or coefficients for biotite at zero ionic strength.

Reactions	log k at 40 °C	log k at 60 °C
$\equiv SOH_2 \rightleftharpoons \, \equiv SOH + H^+$	-5.0 ± 0.2	-5.3 ± 0.1
$\equiv SOH \rightleftharpoons \, \equiv SO^- + H^+$	-7.0 ± 0.3	-6.9 ± 0.2
$\equiv SO^- + Na^+ \rightleftharpoons \, \equiv SONa$	2.0 ± 0.4	3.2 ± 0.1
$\equiv SOH + Na^+ \rightleftharpoons \, \equiv SOHNa^+$	2.0 ± 0.8	2.3 ± 0.2
	log k$_{ex}$ at 40 °C	**log k$_{ex}$ at 60 °C**
$NaX + H^+ \rightleftharpoons HX + Na^+$	2.9 ± 0.2	2.9 ± 0.1

experiments, respectively (see Section 2.1), possibly due to some generation of fine particles during magnetic stirring during titration. Fine particles can have a relatively large SSA and possibly contribute with additional ASD and CEC. Ideally, this could have been verified by performing a particle size analysis of the biotite sample post-titration, either by performing an additional BET analysis, or by determining the particle size before and after titration, using, for example, a Dynamic Light Scattering (DLS) method. Unfortunately, this was not done. However, such additional uptake capacities by fine particles, if present, should not affect the determination of values of reaction constants and coefficients of the biotite mineral, which was the aim of the titration experiments. The optimized values are shown in Table 4.

3.2. Time-dependent batch sorption results

The batch sorption experiments lasted for approximately two months. During this time, the apparent R_d values were expected to increase gradually due to an in-diffusion transport process in the biotite grains. The time-dependent results were comparable for all radioactive elements. Therefore, for illustration purposes only, the time-dependent sorption of barium and cobalt at 0.01 M ionic strength at 25 (Cs, Ba, Co, and Eu sorption onto biotite at pH 5–9 and at varying ionic strength, submitted to J. Environ. Radioactiv.), 40, and 60 °C is presented in Fig. 4. The complete set of time-dependent data for R_d is given in Appendix A in Section A1 (Cs) A2 (Ba), A3 (Co) and A4 (Eu) respectively. The method used for evaluating R_d values from the time-dependent results is detailed in Appendix C, Section A1. The results indicate that the equilibrium for radionuclide sorption was achieved within one month, after which no significant increase in sorption was observed, but rather a slight decrease. The latter may be an effect of partial dissolution of the biotite surface. The rapid increase in sorption during the first month of the batch experiment may be an indication of the presence of a large number of active sites on the biotite surface, while additional sites are

Table 4

Experimental and optimized CEC and ASD values.

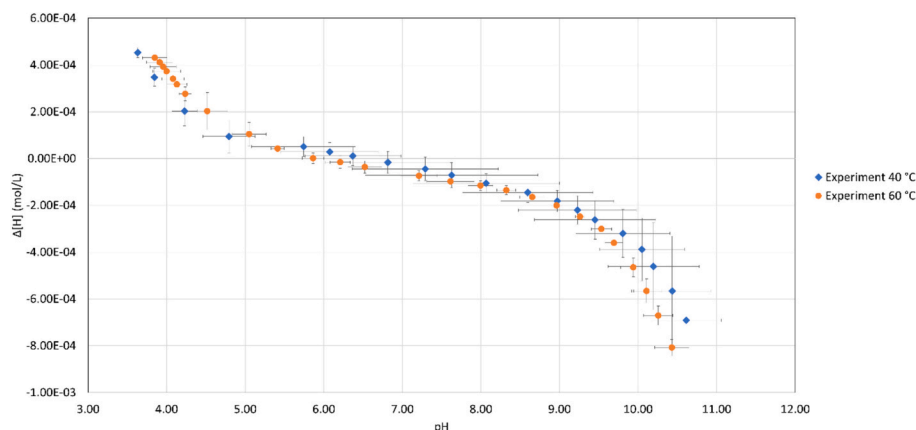|	Experimental value (mol/g)	Optimized value (mol/g)
CEC	$1.0 \pm 0.1 \times 10^{-5}$	$2.5 \pm 0.5 \times 10^{-5}$
ASD	$3.3 \pm 0.6 \times 10^{-6}$	$1.7 \pm 0.1 \times 10^{-5}$

Fig. 3. Potentiometric titration (average of triplicates) of a biotite suspension in 0.01 M NaClO$_4$ solution at 40 and 60 °C.
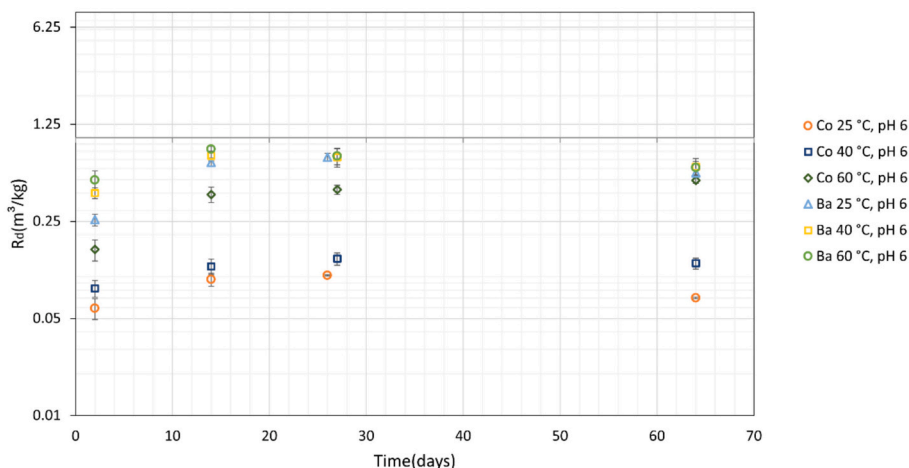
Fig. 4. Example of the effects of contact time on barium and cobalt sorption onto treated biotite for pH 6 in 0.01 M NaClO$_4$ at 25 *(Cs, Ba, Co, and Eu sorption onto biotite at pH 5–9 and at varying ionic strength, submitted to J. Environ. Radioactiv.)*, 40, and 60 °C.

subsequently reached and occupied in the pore system of the particles. Interestingly, the temperature did not seem to have much effect on the time required to reach equilibrium.

Fig. 4 also shows that cobalt sorption increased with rising temperature. However, in the case of barium, temperature had no noticeable effect on its sorption.

3.3. Batch sorption results for Cs

The experimental results for cesium sorption on biotite indicate that all three variables investigated (the ionic strength, pH, and temperature) had significant impacts on the results (see the tables in Appendix A). The R_d values at two months for 0.001, 0.01 and 0.1 M ionic strength are shown in Fig. 5a (40 °C) and 5b (60 °C).

At both temperatures, the R_d values of cesium decrease as the ionic strength increases from 0.001 to 0.1 M, which is most likely an effect of the Na$^+$ ions competing for the accessible sorption sites. In addition, the effect of pH is an increase of the R_d values at both temperatures. The apparent slight decrease in sorption at 0.001 M ionic strength and

temperatures of 40 and 60 °C when the pH increases from 7 to 9 (Fig. 5a, b) is probably within the error margin.

From a comparison of Fig. 5a and b, the temperature has a relatively large positive effect on Cs sorption, with R_d increasing from 2.3 to 7.8 m^3/kg at 0.001 M. For the other two ionic strengths (0.01 M and 0.1 M), the increases in R_d are lesser but still detectable. The temperature effect is the most pronounced for 0.001 M NaClO$_4$ in the pH range of 7–9. One can therefore expect that the surface species that govern cesium sorption under these specific conditions are also responsible for this temperature effect.

The model for Cs enables the following surface species to form: CsX (ion exchange), ≡SOCs ("strong" complex), and ≡SOHCs$^+$ ("weak" complex). However, since the inclusion of the "weak complex" did not to improve the fitting, it was subsequently omitted from model. Fig. 5c and d display the results of Cs sorption modeling for 0.001 M NaClO$_4$ at 40 and 60 °C. The results for 0.01 and 0.1 M are shown in Appendix B. The modeling results suggest that at 40 °C, cesium uptake is primarily governed by ion exchange (CsX) with a contribution from surface complexation (≡SOCs) species across all pH values. In contrast, at 60 °C,
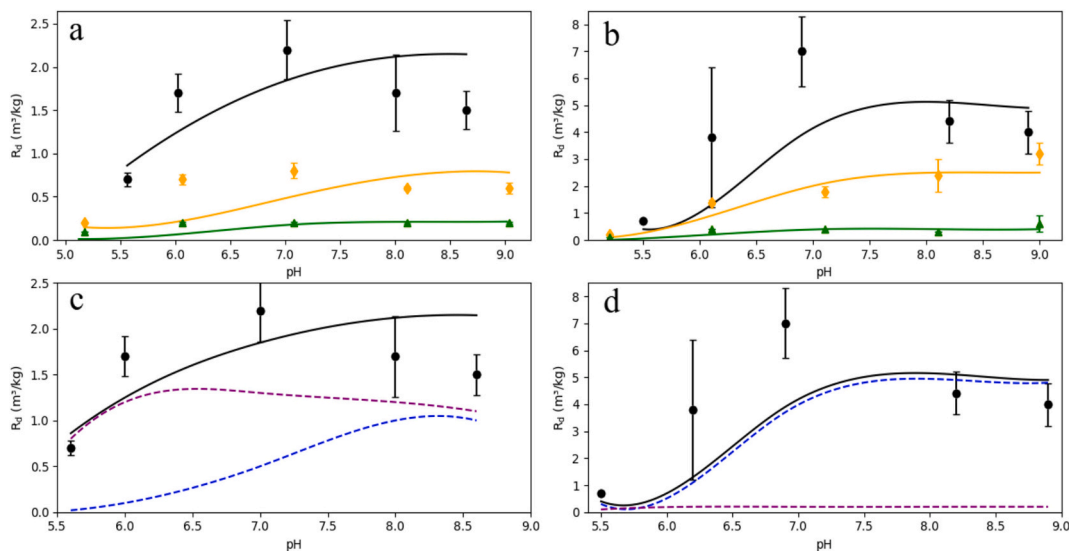

Fig. 5. Experimental (symbols) and modeling (continuous lines) results for cesium sorption onto biotite mineral at 40 °C (a) and 60 °C (b) in 0.001 M (black symbols and lines), 0.01 M (yellow symbols and lines), 0.1 M (green symbols and lines) in NaClO$_4$ solution. The contributions of different Cs species to cesium sorption at 40 (c) and 60 °C (d) for 0.001 M (black symbols and lines) NaClO$_4$ which are CsX (purple dashed line) and ≡SOCs (blue dashed line). (For interpretation of the references to colour in this figure legend, the reader is referred to the web version of this article.)

cesium sorption was only controlled by surface complexation ($\equiv$SOCs) species.

Additionally, at both temperatures, surface complexation becomes the most significant sorption species as the ionic strength increases from 0.001 M to 0.1 M. The ion-exchange species makes a very low (at 40 °C and pH > 6) to negligible (at 60 °C and pH > 5) contribution to sorption, especially at the highest $NaClO_4$ concentration (0.1 M). A summary of the surface reactions and optimized constants and coefficients is given in Table 5.

The modeling results reveal that as temperature increases from 40 °C to 60 °C (Fig. 5) and under the same ionic strength conditions, Cs sorption via ion exchange (CsX) decreases, while surface complexation ($\equiv$SOCs) becomes the predominant mechanism. This shift likely explains the overall increase in cesium sorption with temperature.

Table 5 also shows the selectivity coefficients for cation exchange which were allowed to vary across the three series of different ionic strengths. This variation was allowed because previous studies have shown that the selectivity coefficient seems to be dependent on the ionic strength, see (Missana et al., 2014) and references given therein. However, the results presented here for Cs indicate that this dependence is only marginal with average ion-exchange log k_{ex} values 1.5 ± 0.4 (40 °C) and 0.9 ± 0.1 (60 °C), that is, the standard deviations are acceptable. In conclusion, Cs sorption increased with temperature, especially at low ionic strength at which the competition from Na^+ was low. This effect was ascribed to the formation of the surface complex $\equiv$SOCs. Further, as the temperature increased, surface complexation started to take over as the main sorption process, and at the highest temperature of 60 °C, ion exchange had a very small role in Cs^+ uptake. Besides the temperature effects, both an increased ionic strength and a decreased pH seemed to suppress Cs^+ sorption by Na^+ and H^+ competition mechanisms, respectively.

3.4. Batch sorption results for barium

The experimental and modeling results for R_d values of barium sorption onto biotite for three ionic strengths are presented in Fig. 6a (40 °C) and 6b (60 °C), respectively. The complete set of data is shown in the tables in Appendix A. At both temperatures, the R_d-values of barium are considerably reduced by the increased ionic strength, a behavior similar to that observed for cesium and a result of increased Na^+ competition for the sorption sites.

In addition, Ba sorption clearly indicates that the pH has a significant impact on sorption, with sorption increasing continuously up to pH 9, even though this behavior is suppressed at the highest ionic strength. On the other hand, the increase in temperature from 40 to 60 °C has little effect on sorption, with no significant change in R_d-values, as shown in Fig. 6a and b.

Ba sorption data was initially modelled by considering five sorption

species: BaX_2 and XBaOH (ion-exchange), $\equiv$SOBa$^+$ ("strong" complex), $\equiv$SOHBa^{2+} ("weak" complex), and also the hydrolyzed sorption species $\equiv$SOBaOH. The "weak" complex was subsequently removed from the modeling since it did not improve the fitting of the model to the data. Fig. 6c and d display the modeling results for 0.001 M $NaClO_4$, and the results for 0.01 and 0.1 M are shown in Appendix B. The modeling results indicate that, at 0.001 M $NaClO_4$ and temperatures of 40 and 60 °C sorption is primarily governed by ion exchange, specifically the formation of BaX_2, with additional contributions from surface complexation involving the $\equiv$SOBa$^+$ species across all pH values. However, at pH values greater than 8, some additional contributions from the hydrolyzed surface species, $\equiv$SOBaOH, and XBaOH species were observed.

Furthermore, as the ionic strength increases from 0.001 M to 0.1 M at both temperatures, ion exchange becomes increasingly suppressed, and surface complexation emerges as the dominant sorption mechanism at the highest $NaClO_4$ concentration (0.1 M).

The fact that the ion-exchange surface species BaX_2 is always dominant, except possibly at the highest ionic strength, may explain the lack of temperature dependency of barium sorption. This behavior of barium is in contrast to that of cesium, where the surface complex $\equiv$SOCs was dominant over the ion-exchange species CsX and therefore showed a noticable temperature dependency. From these two cases, one may conclude that surface complexation may be a more temperature-dependent process than ion exchange. A summary of the surface reactions used in the modeling, along with their optimized constants and coefficients, is provided in Table 6.

The surface complexation constant for barium increased with rising temperature, suggesting that the formation of barium surface complexes becomes more pronounced at higher temperatures. The selectivity coefficients for cation exchange were allowed to vary across the series of ionic strengths, and here the large standard deviations of the average results indicate that for barium the coefficients increase with ionic strength, even if they are formally corrected to zero ionic strength, this type of behavior have been discussed previously by (Missana et al., 2014). The average log k_{ex} values for ion exchange for the BaX_2 specie are −0.2 ± 0.5 (40 °C) and 0.5 ± 1.2 (60 °C). In conclusion, the temperature had a small effect on barium sorption. In contrast to the case of cesium, the impact of temperature on barium sorption in 0.001 and 0.01 M $NaClO_4$ solutions was very low at all pH levels. On the other hand, at the highest ionic strength (0.1 M), with ion exchange suppressed, an increase in barium sorption with temperature was seen at high pH levels (pH > 6), However at pH < 6, the impact of temperature was negligible. In contrast to Cs sorption, Ba sorption shows a limited influence from increased temperature. However, similar to the case of Cs, an increased ionic strength and decreased pH suppress barium sorption by Na^+ and H^+ competition mechanisms, respectively. This competition for sorption sites is effective for both surface complexation (Cs) and ion exchange (Ba).

3.5. Batch sorption results for cobalt

The experimental and modeling results for Co sorption onto biotite for three ionic strengths are shown in Fig. 7a (40 °C) and 7b (60 °C), respectively. The complete datasets can be found in Appendix A.

At both temperatures, the R_d values of cobalt are considerably reduced at low pH values, a behavior very similar to those of both cesium and barium and that can be related to increased competition from H^+ for the sorption sites. However, unlike Cs and Ba, the effect of increased ionic strength is comparatively small or reversed, with increasing sorption with ionic strength. The temperature has a relatively large positive effect on Co sorption. These findings could be an indication of the formation of strong cobalt surface complexes on the biotite surface. Another feature so far unique for Co is that sorption increases from pH 6 to 8 and then begins to decline from pH 8 to 9 for all three ionic strengths and at both 40 and 60 °C. This type of declining sorption with pH is typical for elements that are strongly hydrolyzed.

Table 5

Surface complexation and cation-exchange reactions and their associated constants (log k) and selectivity coefficients (log k$_{ex}$) for Cs at 40 and 60 °C at zero ionic strength.

Reactions	log k (40 °C)	log k (60 °C)
$\equiv$SO$^-$ + Cs$^+$ ⇌ $\equiv$SOCs	5.0 ± 0.2	6.2 ± 0.2
$\equiv$SOH + Cs$^+$ ⇌ $\equiv$SOHCs$^+$	Not significant*	Not significant*

Reaction/ ionic strength at 40 °C	log k$_{ex}$ (0.001 M)	log k$_{ex}$ (0.01 M)	log k$_{ex}$ (0.1 M)
Cs$^+$ + NaX ⇌ CsX + Na$^+$	1.8	1.7	1.0

Reaction/ionic strength at 60 °C			
Cs$^+$ + NaX ⇌ CsX + Na$^+$	0.9	1.0	0.8

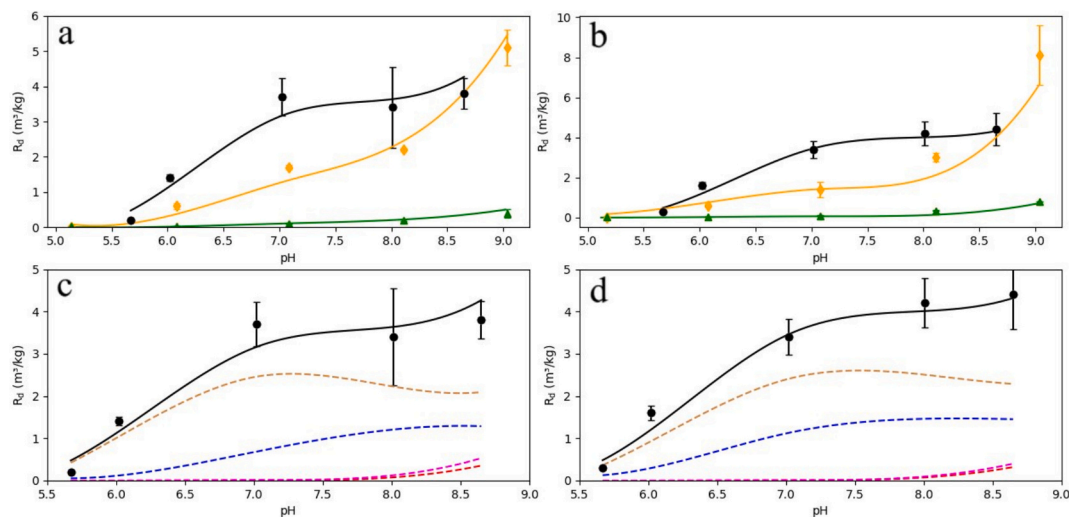* The surface complex did not improve the fitting of the model.

Fig. 6. Experimental (symbols) and modeling (continuous lines) results for barium sorption onto biotite mineral at 40 °C (a) and 60 °C (b) in 0.001 M (black symbols and lines), 0.01 M (yellow symbols and lines), 0.1 M (green symbols and lines) in NaClO₄ solution. The contributions of different Ba species to barium sorption at 40 °C (c) and 60 °C (d) for 0.001 M (black symbols and lines) NaClO₄ are: BaX₂ (gold dashed line), $\equiv$SOBa^+; (blue dashed line), $\equiv$SOBaOH (red dashed line) and XBaOH, (magenta dashed line). (For interpretation of the references to colour in this figure legend, the reader is referred to the web version of this article.)

Table 6

Surface complexation and cation-exchange reactions and their associated constants (log k) for Ba at 40 and 60 °C at zero ionic strength.

Reaction	log k (40 °C)	log k (60 °C)
$\equiv SO^- + Ba^{2+} \rightleftharpoons \equiv SOBa^+$	5.3 ± 0.3	5.9 ± 0.4
$\equiv SO^- + Ba(OH)^+ \rightleftharpoons \equiv SOBaOH$	9.3 ± 0.3	9.7 ± 1.1
$\equiv SOH + Ba^{2+} \rightleftharpoons \equiv SOHBa^{2+}$	Not significant*	Not significant*
	6.1 ± 0.5	5.2 ± 0.3

Reaction/Ionic Strength at 40 °C	log k$_{ex}$ (0.001 M)	log k$_{ex}$ (0.01 M)	log k$_{ex}$ (0.1 M)
NaX + BaOH$^+$⇌BaOHX + Na$^+$	5.8	6.7	6.0
Ba^{2+} + 2NaX⇌BaX$_2$ + 2Na$^+$	$-$ 0.5	0.3	1.2

Reaction/Ionic Strength at 60 °C			
NaX + BaOH$^+$⇌BaOHX + Na$^+$	5.0	5.1	5.6
Ba^{2+} + 2NaX⇌BaX$_2$ + 2Na$^+$	$-$ 0.6	0.5	0.7

* Inclusion did not improve the fitting of the model to the sorption data.

In order to fit a model to the Co sorption data, three surface complexes ($\equiv$ SOCo$^+$, $\equiv$ SOCoOH, $\equiv$ SOCo(OH)$_2^-$) and one ion-exchange species (CoX₂) were considered but the latter specie contribution to sorption was found to be negligible. Also, the weak surface complex $\equiv$ SOHCo^{2+} was found to play a negligible role and was therefore excluded from the modeling. Figs. 7c (40 °C) and 7d (60 °C) display the modeling results for 0.001 M NaClO₄, and those for 0.01 and 0.1 M are shown in Appendix B. The modeling results indicate that Co sorption at pH 7 is primarily governed by the $\equiv$ SOCo$^+$ species but already at pH 8, $\equiv$ SOCoOH becomes the dominant sorbing species with the $\equiv$ SOCo(OH)$_2^-$ species also contributing at highest pH. The surface complexation reactions that were used are listed in Table 7, along with their optimized constants.

Cobalt sorption modeling results show a predominant surface complexation mechanism, which should be in line with the reasoning above regarding a correlation between surface complexation and a strong influence from temperature changes. Co shows a particular strong effect from temperature (Fig. 7a and b) with the maximum R_d value, at approximately pH 7–8, increasing from 8 to 19 m^3/kg for 0.1 M NaClO₄

and significantly, the reaction constants for all Co surface complexes increase with temperature (Table 7). In conclusion, cobalt sorption increased with temperature at all three ionic strengths investigated. This effect was ascribed to the formation of three surface complexes $\equiv$SOCo$^+$, $\equiv$ SOCoOH, and $\equiv$ SOCo(OH)$_2^-$. The sorption of cobalt was unique among the elements investigated in this study in that sorption was modelled purely as surface complexation without any involvement of ion exchange. The observed decrease in sorption for cobalt above pH 8 is likely due to the formation of aqueous hydroxide complexes. At low pH, cobalt sorption decreased rapidly, most likely due to the protonation of the surface complexation sites.

3.6. Batch sorption results for europium

The modeling and experimental data for Eu sorption at all ionic strengths (0.001, 0.01, and 0.1 M) at are shown in examples Fig. 8a (40 °C) and 8b (60 °C). The complete dataset is shown in Appendix A.

Europium sorption increases as the pH increases to approximately pH 6–7 at both temperatures and then gradually decreases as the pH increase further. The decrease is most likely attributed to the formation of aqueous Eu hydroxyl complexes. The influence of ionic strength is not particularly pronounced. The temperature has a comparatively large positive effect on europium sorption, increasing R_d from approximately 11 to 35 m^3/kg for 0.01 M NaClO₄ at pH 6. When comparing Eu sorption results with the results for the other three elements, this indicates that Eu sorption, much like Cs, is governed by a mixture of surface complexation and ionic strength. Compared with Cs, however, the complexity of its sorption behavior is increased by the formation of hydrolyzed species. Eu sorption was modelled by considering three surface complexation species: $\equiv$ SOEu^{2+}, $\equiv$ SOEu(OH)$^+$, $\equiv$ SOEu(OH)$_2$, and one ion-exchange species EuX₃. The other species considered was a weak surface complex ($\equiv$ SOHEu$^+$), but it had a negligible contribution to the model fitting and thus was later excluded from the modeling. The data fitting results for the case of 0.001 M NaClO₄ at and are shown in Fig. 8c (40 °C) and 8d (60 °C) respectively. The results for 0.01 and 0.1 M NaClO₄ can be found in Appendix B. The data for 40 °C (Fig. 8c) indicate that at a pH of approximately 5, the sorption is dominated by the ion-exchange species EuX₃. However, when the pH increases, the europium uptake is chiefly governed by surface complexation species $\equiv$ SOEu^{2+} and $\equiv$ SOEu(OH)$^+$. This phenomenon is probably related to the pK_{a2} value of approximately 7 for biotite. At 60 °C (Fig. 8d), the
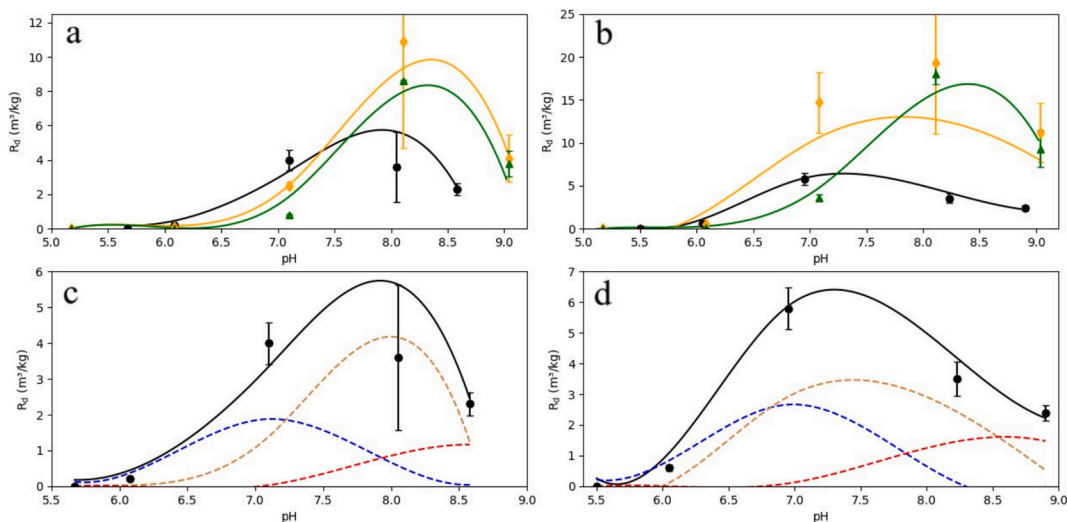
Fig. 7. Experimental (symbols) and modeling (continuous lines) results for cobalt sorption onto biotite mineral at 40 °C (a) and 60 °C (b) in 0.001 M (black symbols and lines), 0.01 M (yellow symbols and lines), 0.1 M (green symbols and lines) in NaClO$_4$ solution. The contributions of different Co species to cobalt sorption at 40 °C (c) and 60 °C (d) for 0.001 M (black symbols and lines) NaClO$_4$ are represented by different curves: $\equiv SOCo^+$ (blue dashed line) $\equiv$ SOCoOH (gold dashed line) and $\equiv SOCo(OH)_2^-$ (red dashed line). (For interpretation of the references to colour in this figure legend, the reader is referred to the web version of this article.)

Table 7

Modelled surface complexation reactions and their associated constants (log k) for Co at 40 and 60 °C at zero ionic strength.

Reaction	log k (40 °C)	log k (60 °C)
$\equiv SO^- + Co^{2+} \rightleftharpoons \equiv SOCo^+$	5.6 ± 0.4	6.4 ± 0.4
$\equiv SO^- + Co(OH)^+ \rightleftharpoons \equiv SOCoOH$	8.0±0.7	8.3 ± 1.0
$\equiv SO^- + Co(OH)_2 \rightleftharpoons \equiv SOCo(OH)_2^-$	5.7±0.6	6.7±1.3
$\equiv SOH + Co^{2+} \rightleftharpoons \equiv SOHCo^{2+}$	Not significant*	Not significant*
$Co^{2+} + 2NaX \rightleftharpoons CoX_2 + 2Na^+$	Not significant*	Not significant*

* Inclusion did not improve the fitting of the model to sorption data.

modeling results suggest that for all three ionic strengths, at a pH of approximately 6, the exchange species EuX$_3$ is completely suppressed, and sorption is dominated by surface complexation and especially by

$\equiv SOEu^{2+}$. Apparently, this surface complex is enhanced over the other surface species by the increased temperature. The surface complexation reactions that were used are listed in Table 8, along with their optimized constants.

Similar to Cs, Ba, and Co, the surface complexation constant for Eu was found to increase with temperature (Table 8), indicating a greater tendency for Eu surface complexation species to form. The selectivity coefficient for EuX$_3$ species was allowed to vary with ionic strength, as shown in Table 8. Similar to what was found for the Ba exchange reaction, the relatively large variation indicates that this parameter is not independent of ionic strength, instead the coefficients shows an increasing trend with ionic strength. The effect of temperature on the coefficients is, on the other hand, negligible.
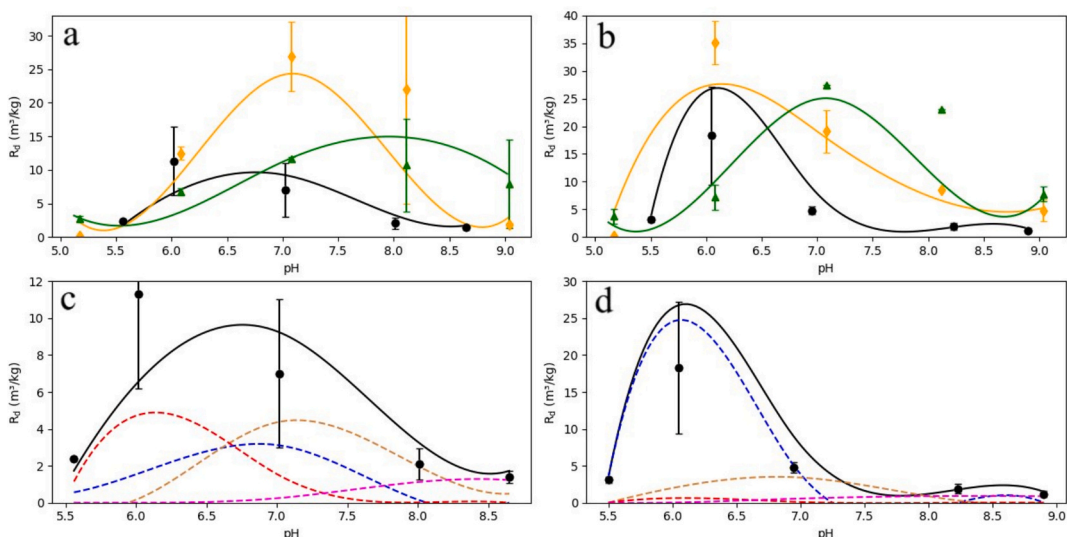

Fig. 8. Experimental (symbols) and modeling (continuous lines) results for europium sorption onto biotite mineral at 40 °C (a) and 60 °C (b) in 0.001 M (black symbols and lines), 0.01 M (yellow symbols and lines), 0.1 M (green symbols and lines) in NaClO$_4$ solution. The contributions of different Eu species to europium sorption at 40 °C (c) and 60 °C (d) for 0.001 M (black symbols and lines) NaClO$_4$ are represented by different curves:: EuX_3 (red dashed line), $\equiv SOEu^{2+}$ (blue dashed line), $\equiv SOEu(OH)^+$ (gold dashed line) and $\equiv SOEu(OH)_2$. (magenta dashed line). (For interpretation of the references to colour in this figure legend, the reader is referred to the web version of this article.)

Table 8

Surface complexation and cation-exchange reactions and their associated constants (log k) and exchange coefficients for Eu.

Reaction	log k (40 °C)		log k (60 °C)
$\equiv SO^- + Eu^{3+} \rightleftharpoons \equiv SOEu^{2+}$	6.5 ± 0.8		8.1 ± 0.2
$\equiv SO^- + Eu(OH)^{2+} \rightleftharpoons \equiv SOEu(OH)^+$	6.9 ± 1.3		8.1 ± 1.2
$\equiv SO^- + Eu(OH)_2^+ \rightleftharpoons \equiv SOEu(OH)_2$	5.6 ± 1.2		6.6 ± 1.2
Reaction/Ionic Strength at 40 °C	**log k$_{ex}$ 0.001 M**	**log k$_{ex}$ 0.01 M**	**log k$_{ex}$ 0.1 M**
$Eu^{3+} + 3NaX \rightleftharpoons EuX_3 + 3Na^+$	-2.7	0.3	3.3
Reaction/Ionic Strength at 60 °C	**0.001 M**	**0.01 M**	**0.1 M**
$Eu^{3+} + 3NaX \rightleftharpoons EuX_3 + 3Na^+$	-2.9	-0.2	3.1

3.7. Modeling of thermodynamic parameters

Using the van't Hoff formalism, the thermodynamic parameters of enthalpy and entropy of reaction can be deduced by plotting the temperature dependence of the reaction constant or coefficient ((log K) vs. 1/T) by using Eq. (10). All ion exchange coefficients were taken as average values, even if some variation with ionic strength was found. The plot of the log K values, obtained from previous sections of modeling of the experimental R_d values at different temperatures, vs. 1/T was a straight line with a gradient of $-\Delta H^o/R$ and an intercept of $\Delta S^o/R$. Thus, the enthalpy and entropy of the reactions were constant in the investigated temperature range, as illustrated in Fig. 9. The dataset shown in this figure is extended with the constants determined at 25 °C in another work (Cs, Ba, Co, and Eu sorption onto biotite at pH 5–9 and at varying ionic strength, submitted to J. Environ. Radioactiv.). Table 9 shows ΔH^o and ΔS^o for the sorption reactions of all elements based on the ion-exchange and surface complexation constants, as discussed above.

The results in Table 9 show that both the enthalpy and entropy for the cesium, barium, cobalt, and europium surface complexes are positive. The Gibbs free energy is negative, (K>1) implying that the surface complexes are spontaneous reactions and entropy-driven, which can be attributed to the formation of the inner sphere complex, where the hydration shell of the adsorbing species is at least partially released. In general, cations are very well solvated in water. In order to sorb these ions on mineral surfaces, the dehydration of water molecules from the cation is required. The enthalpy values calculated from the temperature-dependent equilibrium constants (Table 9) for the sorption reaction are

Table 9

Thermodynamic parameters for the sorption of cesium, barium, cobalt, and europium onto biotite.

Surface complex/ion-exchange species for elements	$\Delta H^0 \left(kJ\,mol^{-1} \right)$	$\Delta S^0 \left(JK^{-1}mol^{-1} \right)$
Cesium		
$\equiv SOCs$	38.1	164.8
CsX	-18.6	-47.9
Barium		
$\equiv SOBa^+$	20.9	111.6
$\equiv SOBaOH$	12.4	117.6
BaX_2	-6.3	-17.2
$XBaOH$	-46.1	-95.4
Cobalt		
$\equiv SOCo^+$	22.6	119.9
$\equiv SOCoOH$	23.5	140.4
$\equiv SOCo(OH)_2^-$	45.3	191.8
Europium		
$\equiv SOEu^{2+}$	8.3	76.4
$\equiv SOEuOH^+$	43.0	195.6
$\equiv SOEu(OH)_2$	32.2	150.9
EuX_3	-9.6	-28.7

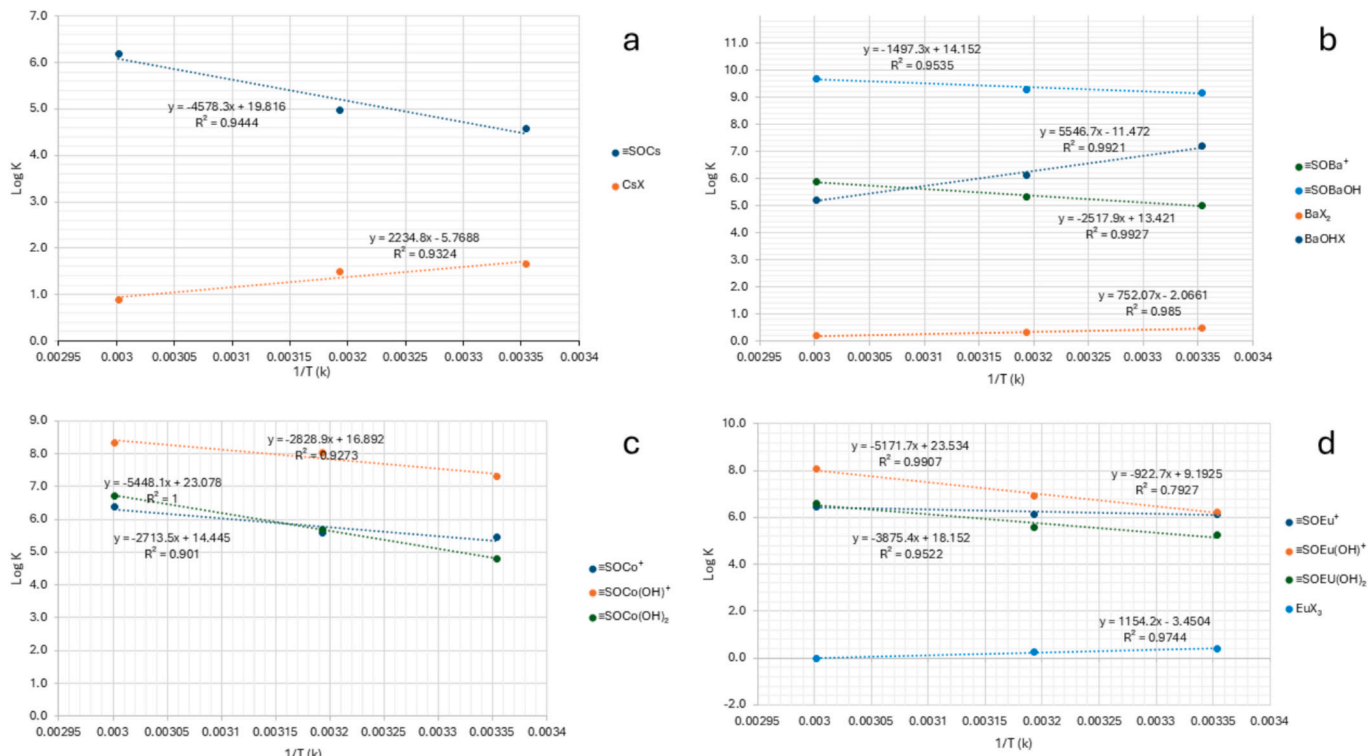**Fig. 9.** Van't Hoff plots of the calculated surface complexation constants and ion-exchange coefficients for ^{134}Cs (a), ^{133}Ba (b), ^{60}Co (c) and ^{152}Eu (d).

endothermic (heat-adsorbing), which means that a significant quantity of energy is necessary for the partial de-solvation of the cations during the formation of the inner sphere complex. During this process, water molecules are released from the hydration sphere, resulting in positive entropy.

On the other hand, the enthalpy values for the exchange surface species CsX, BaX$_2$, XBaOH, and EuX$_3$ species were determined to -18.6, -6.3, -46.1, and -9.6 JK^{-1}mol^{-1}, respectively and consequently exothermic (heat-releasing). The negative enthalpy values for CsX, BaX$_2$, XBaOH, and EuX$_3$, which are in contrast with the positive enthalpy values for the other surface complexes, as outlined above, could be explained by the hypothesis that these species are indeed of the ion-exchange type, which need minimal cation dehydration before sorbing on the cation-exchange site of biotite and hence have a little effect on entropy. Instead, the exchange is probably driven by the exothermic replacement of Cs$^+$, Ba^{2+}, and Eu^{3+} in solution by Na$^+$, which is a much better solvated cation than the other three cations. That ion-exchange is mainly a solvation-promoted process rather than an adsorption-promoted process have been demonstrated with combined microcalorimetry and modeling studies by (Rotenberg et al., 2009).

4. Conclusions

A batch sorption experiment was conducted to investigate the sorption of ^{134}Cs, ^{133}Ba, ^{60}Co, and ^{152}Eu in a mixture at trace concentrations on sodium-converted biotite. The experiment was conducted in triplicates at pH 5–9 with background electrolytic solutions containing 0.001, 0.01, and 0.1 M NaClO$_4$ at 40 and 60 °C. All elements were considerably affected by the pH, but the ionic strength affected mainly Cs and Ba and to some extent also Eu. The temperature-dependence study showed that the sorption of Cs, Co, and Eu was influenced by temperature; however, Ba sorption showed little dependence on temperature. The modeling suggests that this behavior can be explained by formation of both surface complexes and ion-exchange species. Surface complexation shows a strong temperature dependency, while the effect on ion exchange is comparatively low. The temperature dependencies of the modelled reaction constants and coefficients can be used to verify the type of binding to the surface. This ability represents a certain advantage of this approach over spectroscopic methods that are used to identify sorption mechanisms because the latter usually operate at much higher sorbing element concentrations. The temperature variation method, on the other hand, works under exactly the same conditions as those under which the binding constants are determined. For the ion-exchange species, a negative enthalpy was calculated, which shows that these species may undergo sorption on the biotite surface via a solvation process. The surface complexes, on the other hand, had positive enthalpy, which implies that the surface complexation reactions are endothermic and entropically driven. The positive enthalpy of the complexes may indicate that they undergo sorption onto the mineral surface by shedding their hydration layer, forming an inner-sphere complex.

CRediT authorship contribution statement

Pawan Kumar: Writing – original draft, Software, Methodology, Formal analysis, Data curation, Conceptualization. **Stellan Holgersson:** Writing – review & editing, Supervision, Methodology, Funding acquisition, Formal analysis, Data curation, Conceptualization. **Christian Ekberg:** Writing – review & editing, Supervision, Methodology, Funding acquisition, Data curation, Conceptualization.

Declaration of competing interest

The authors declare the following financial interests/personal relationships which may be considered as potential competing interests:
Pawan Kumar reports financial support was provided by Swedish

Appendix A. Supplementary data

Supplementary data to this article can be found online at https://doi.org/10.1016/j.jconhyd.2025.104593.

Data availability

Data will be made available on request.

References

Allard, B., Beall, G.W., 1979. Sorption of americium on geologic media. J. Environ. Sci. Heal. A 14, 507–518.

Allard, B., Beall, G.W., Krajewski, T., 1980. The sorption of actinides in igneous rocks. Nucl. Technol. 49, 474–480.

Andersson, M., et al., 2008. Development of Methodology for Evaluation of Long-Term Safety Aspects of Organic Cement Paste Components (WR-08-28). Posiva Oy, Olkiluoto.

Berubé, Y.G., Onoda, G.Y., De Bruyn, P.L., 1967. Proton adsorption at the ferric oxide/aqueous solution interface. Surf. Sci. 8, 448–461.

Bradbury, M.H., Baeyens, B., 2000. A generalized sorption model for the concentration dependent uptake of caesium by argillaceous rocks. J. Contam. Hydrol. 42, 141–163.

Brunauer, S., Emmet, P.H., Teller, E., 1938. Adsorption of gases in multimolecular layers. J. Am. Chem. Soc. 60, 309–319.

Charlton, S.R., Parkhurst, D.L., 2011. Modules based on the geochemical model PHREEQC for use in scripting and programming languages. Comput. Geosci. 37, 1653–1663.

Cornell, R.M., 1993. Sorption of cesium on minerals: a review. J. Radioanal. Nucl. Ch. 171, 483–500.

Crawford, J., 2010. Bedrock Kd Data and Uncertainty Assessment for Application in SR-Site Geosphere Transport Calculations (R-10-48). Svensk Kärnbränslehantering AB, Stockholm.

Davis, J.A., Coston, J.A., Kent, D.B., Fuller, C.C., 1998. Application of the surface complexation concept to complex mineral assemblages. Environ. Sci. Technol. 32, 2820–2828.

Davis, J.A., Meece, D.E., Kohler, M., Curtis, G.P., 2004. Approaches to surface complexation modeling of uranium(VI) adsorption on aquifer sediments. Geochim. Cosmochim. Acta 68, 3261–3641.

Drake, H., Sandström, B., Tullborg, E.-L., 2006. Mineralogy and Geochemistry of Rocks and Fracture Fillings from Forsmark and Oskarshamn: Compilation of Data for SR-Can (R-06-109). Svensk Kärnbränslehantering AB, Stockholm.

Ekberg, C., Brown, P.L., 2016. Hydrolysis of Metal Ions, vol. 1 and 2. Wiley-VCH, Weinheim, Germany.

Ewing, R., 2015. Long-term storage of spent nuclear fuel. Nat. Mater. 14, 252–257.

Fabritius, O., et al., 2022. Radium sorption on biotite; surface complexation modeling study. Appl. Geochem. 140, 105289.

Fukushi, K., et al., 2013. Sorption of Eu(III) on granite: EPMA, LA-ICP-MS, batch and modeling studies. Environ. Sci. Technol. 47, 12811–12818.

Furuya, K., et al., 1997. Sorption of plutonium on a biotite mineral. Sci. Rep. RITU A 45, 89–91.

Gran, G., 1950. Determination of the equivalent point in potentiometric titrations. Acta Chem. Scand. 4, 557–559.

Grisak, G.E., Pickens, J.F., 1980. Solute transport through fractured media: 1. The effect of matrix diffusion. Water Resour. Res. 16, 719–730.

Hakanen, M., Ervanne, H., Puukko, E., 2012. Safety Case for the Disposal of Spent Nuclear Fuel at Olkiluoto - Radionuclide Migration Parameters for the Geosphere (POSIVA 2012–41). Posiva Oy, Olkiluoto, Finland.

Hedin, A., Olsson, O., 2016. Crystalline rock as a repository for Swedish spent nuclear fuel. Elements 247–252.

Holgersson, S., Kumar, P., 2023. A literature review on thermodynamic sorption models of radionuclides with some selected granitic minerals. Front. Nucl. Eng. 2, 1227170.

Holgersson, S., Drake, H., Karlsson, A., Krall, L., 2024. Biotite dissolution kinetics at pH 4 and 6.5 under anaerobic conditions and the release of dissolved Fe(II). Chem. Geol. 662, 122204.

Idemitsu, K., Obata, K., Furuya, H., Inagaki, Y., 1994. Sorption behavior of uranium (VI) on a biotite mineral. Mater. Res. Soc. Symp. P. 353, 981–988.

IIda, Y., Yamaguchi, T., Tanaka, T., Hemmi, K., 2016. Sorption behavior of thorium onto granite and its constituent minerals. J. Nucl. Sci. Technol. 53, 1573–1584.

Jakobsson, A.-M., 1999. Measurement and Modelling Using Surface Complexation of Cation (II to VI) Sorption onto Mineral Oxides. Chalmers University of Technology, Department of Nuclear Chemistry, Göteborg.

Jordan, N., et al., 2024. A critical review of the solution chemistry, solubility, and thermodynamics of europium: recent advances on the Eu(III) hydrolysis. Coord. Chem. Rev. 510, 215702.

Kyllönen, J., et al., 2014. Modeling of cesium sorption on biotite using cation exchange selectivity coefficients. Radiochim. Acta 102, 919–929.

McKinley, J.P., et al., 2004. Microscale distribution of cesium sorbed to biotite and muscovite. Environ. Sci. Technol. 38, 1017–1023.

Missana, T., Benedicto, A., Garcia-Gutierrez, M., Alonso, U., 2014. Modeling cesium retention onto Na-, K- and Ca-smectite: effects of ionic strength, exchange and competing cations on the determination of selectivity co-efficients. Geochim. Cosmochim. Ac. 128, 266–277.

Murali, M.S., Mathur, J.N., 2002. Sorption characteristics of Am(III), Sr(II) and Cs(I) on bentonite and granite. J. Radioanal. Nucl. Ch. 254, 129–136.

Muuri, E., et al., 2016. Bahavior of Cs in Grimsel granodiorite: sorption on main minerals and crushed rock. Radiochim. Acta 104, 575–582.

Nagy, K.L., 1995. Dissolution and precipitation kinetics of sheet silicates. Rev. Mineral. Geochem. 31, 173–233.

Nebelung, C., Brendler, V., 2010. U(VI) sorption on granite: prediction and experiments. Radiochim. Acta 98, 621–625.

Nelder, J.A., Mead, R., 1965. A simplex method for function minimization. Aust. Comput. J. 7, 308–313.

Neretnieks, I., 1980. Diffusion in the rock matrix: an important factor in radionuclide retardation. J. Geophys. Res-Sol. Ea. 85, 4379–4397.

Ohe, T., 1984. Ion-exchange adsorption of radioactive cesium, cobalt, manganese and strontium to granitoid rocks in the presence of competing cations. Nucl. Technol. 67, 92–101.

Parkhurst, D.L., Appelo, C.A.J., 2021. PHREEQC Version 3: Computer Program for Speciation, Batch-Reaction, One-Dimensional Transport, and Inverse Geochemical Calculations [Software]. U.S. Geological Survey, s.l.

Payne, T.E., et al., 2013. Guidelines for thermodynamic sorption modelling in the context of radioactive waste disposal. Environ. Model. Softw. 42, 143–156.

Puukko, E., et al., 2007. Sorption of nickel and europium on biotite. In: 3rd Annual Workshop Proceedings -6th EC FP-FUNMIG IP. Nuclear Decommisioning Authority, Moor Row, UK.

Rieder, M., et al., 1998. Nomenclature of the micas. Clay Clay Miner. 46, 586–595.

Rodionova, A.A., Petrov, V.G., Vlasova, I.E., 2022. Sorption of np, Pu, am, St, Cs on mineral phases of the rocks of the Nizhnekansky granitoid massif under conditions of underground repositories for radioactive wastes. Radiochemistry 64, 740–749.

Rotenberg, B., et al., 2009. On the driving force of cation exchange in clays: insights from combined microcalorimetry experiments and molecular simulation. Geochim. Cosmochim. Ac. 73, 4034–4044.

Schollenberger, C., Simon, R., 1945. Determination of exchange capacity and exchangeable bases in soil—ammonium acetate method. Soil Sci. 59, 13–24.

Selnert, E., Byegård, J., Widestrand, H., 2008. Forsmark Site Investigation - Laboratory Measurements within the Site Investigation Programme for the Transprt Properties of the Rock, Final Report (P-07-139). Svensk Kärnbränslehantering AB, Stockholm.

Skagius, K., Svedberg, G., Neretnieks, I., 1982. A study of strontium and cesium sorption on granite. Nucl. Technol. 59, 302–313.

SKB, 2010a. Design and Production of the KBS-3 Repository (TR-10-12). Svensk Kärnbränslehantering AB, Stockholm.

SKB, 2010b. Radionuclide Transport Report for the Safety Assessment SR-Site (TR-10-50). Svensk Kärnbränslehantering AB, Stockholm.

SKB, 2010c. Spent Nuclear Fuel for Disposal in the KBS-3 Repository (TR-10-13). Svensk Kärnbränslehantering AB, Stockholm.

SKB, 2011. Long-Term Safety for the Final Repository for Spent Nuclear Fuel at Forsmark, Main Report of the SR-Site Project, Vol. I-III. Svensk Kärnbränslehantering AB, Stockholm (TR-11-01).

SKBF/KBS, 1983. Kärnbränslecykelns slutsteg. Svensk Kärnbränsleförsörjning AB (Swedish Nuclear Fuel and Waste Management Company, Stockholm.

Söderlund, M., Ervänne, H., Muuri, E., Lehto, J., 2019. The sorption of alkaline earth metals on biotite. Geochem. J. 53, 223–234.

Tachi, Y., et al., 2015. Matrix diffusion and sorption of Cs, Na, I and HTO in granodiorite: laboratory-scale results and their extrapolation to the in situ conditions. J. Contam. Hydrol. 179, 10–24.

Tsai, S.-C., et al., 2009. Cesium adsorption and distribution onto crushed granite under different physicochemical conditions. J. Hazard. Mater. 161, 854–861.

Wissmeier, L., Barry, D.A., 2011. Simulation tool for variably saturated flow with comprehensive geochemical raction in the two and three dimensional domains. Env. Modell. Softw. 26, 210–218.

Yu, Q., Kandegedara, A., Xu, Y., Rorabacher, D.B., 1997. Avoiding interferences from good's buffers: a contiuous series of noncomplexing tertiary amine buffers covering the entire range of pH 3-11. Anal. Biochem. 253, 50–56.